Acoust. Sci. & Tech. **27**, 3 (2006)

PAPER

Numerical simulation of unsteady flow through the rigid glottis

Hideyuki Nomura* and Tetsuo Funada

Graduate School of Natural Science and Technology, Kanazawa University, Kakuma-machi, Kanazawa, 920–1192 Japan

(*Received 24 June 2005, Accepted for publication 24 October 2005*)

Abstract: The present study is intended as an investigation of speech dynamics, particularly the unsteady motion of glottal flow in the larynx. In order to focus on only fluid motion, the vocal cords are assumed to be non-vibrating rigid bodies, although the glottal sound source is described as the interaction between the flow and the vibrating vocal cords. The glottal flow based on the two-dimensional rigid body model is simulated by solving basic equations in a compressible viscous fluid that is subject to appropriate initial and boundary conditions. The obtained results demonstrate that the initial glottal flow was a simple symmetric jet and that the flow became an unsteady complicated flow with vortices distributed in two-dimensional space. Furthermore, the structure of the complicated flow changed with time. These results indicate that simple assumptions, such as linearization of the fluid equations or one-dimensional models, are inappropriate for analysis of the speech production process.

Keywords: Speech production, Glottal flow, Rigid glottal model, Unsteady flow, Numerical simulation

PACS number: 43.70.Aj, 43.70.Bk [DOI: 10.1250/ast.27.154]

1. INTRODUCTION

A better understanding of the dynamics of the speech production process may help to improve the quality of voice synthesis or contribute to the treatment of voice disorders.

Several studies have investigated model analysis of the speech production process. Ishizaka and Flanagan [1] have proposed a well-known two-mass model as a sound source model, and improvement models of that, for example, a three-mass model [2] and a single mass model with two degrees of freedom in the direction parallel and perpendicular to the main flow [3], were proposed. Although the structure of the two-mass model is simple, this model can be used to describe the principal mechanisms of phonation. The glottal flow in the two-mass model is assumed to be a one-dimensional quasi-steady state flow in order to simplify analysis. In addition, the pressure drop in the convergent part of the glottis is described by an experimentally obtained formula reported by van den Berg *et al.* [4], and the pressure increase in the supraglottal region is described using a formula that was derived under the assumption of a steady flow under sudden expansion.

On the other hand, flows through the glottis based on a physical glottal model have been measured in order to clarify complicated phenomena in the larynx. The measurements have indicated jet-like unsteady and asymmetric flows with several vortices, which cause turbulent noises [5–9]. However, very few attempts have been made to theoretically or numerically explain such unsteady or asymmetrical glottal flows obtained experimentally. Iijima *et al.* [10] and Liljencrants [11] have conducted detailed numerical analyses of the pressure distributions in a two-dimensional static glottis based on fluid dynamics assumed an incompressible fluid for the glottal flow. Although their results suggested that the shape of the glottis affects the pressure distribution in the larynx, experimentally obtained results for unsteady or asymmetric flows could not be confirmed using their analyses.

The purpose of the present study is to clarify the dynamics of the speech production process, in particular, the unsteady behavior and nonlinear motion of the glottal flow in phonation. In general, the glottal flow and the vocal cords interact. In the present study however, as a first step, we do not consider this interaction, because our focus is only on fluid motion. The present paper describes numerical simulations of the glottal flow based on a static glottal model and prediction of the experimentally obtained results for asymmetrical or unsteady flows is attempted. From the results, we indicate that the assumption of one-dimensional or symmetric flows in the larynx are not appropriate for analyses of the speech production process, due to the com-

*e-mail: nomu@t.kanazawa-u.ac.jp

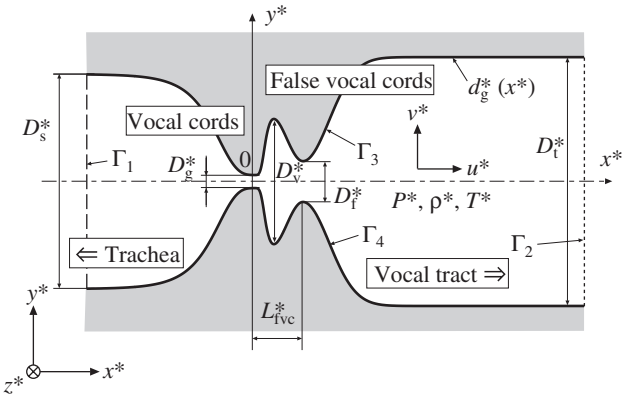

Fig. 1 Rigid glottal model.

plicated nature of such flows. Furthermore, the asymmetric glottal flow obtained herein by computation is not caused by numerical errors and represents valid physical phenomena.

2. ANALYTICAL MODEL

2.1. Rigid Glottal Model

A rigid model without vibration is shown in Fig. 1. In order to formulate the problems, we shall introduce the following nondimensional variables:

$$t = \frac{c_0^* t^*}{D^*}, \quad x = \frac{x^*}{D^*}, \quad y = \frac{y^*}{D^*},$$
$$u = \frac{u^*}{c_0^*}, \quad v = \frac{v^*}{c_0^*}, \quad P = \frac{P^*}{\rho_0^* c_0^{*2}}, \quad T = \frac{T^*}{T_0^*}, \qquad (1)$$

where t is the time, x and y are the spatial coordinates, u and v indicate the x and y components, respectively, of the flow velocity vector $\boldsymbol{u}$, P is the total pressure, ρ is the density of the medium, and T is the absolute temperature. Furthermore, $D^* = D_t^*$ is a characteristic length, and c_0^* is the sound velocity of infinitesimal amplitude. In this paper, all variables denoted by * are dimensional values, and the subscript $_0$ designates quantities at an atmospheric pressure of 1 atm and a temperature of $T^* = 310.15\,\mathrm{K}$ ($= T_0^*$, 37°C).

The configuration is symmetric about the center line (dot-dashed line, i.e. the x^* axis) and uniform in the z^* direction in Fig. 1. In other words, we assume that the glottis can be approximated by a symmetrical two-dimensional rigid channel.

The shape of the glottis is described by the function $d_g^*(x^*)$. Based on the models of Zhang *et al.* [12] and Scherer *et al.* [13], the glottal shape function is written as

$$d_g^*(x^*) = d_{vc}^*(x^*) + d_{fvc}^*(x^*), \qquad (2)$$

$$d_{vc}^*(x^*) = \frac{1}{2}\{A_1^* + A_2^* + (A_1^* - A_2^*)\tanh s(x^*)\}, \qquad (3)$$

$$d_{fvc}^*(x^*) = \begin{cases} 0 & (x^* < L_{fvc}^* - \Delta L_{fvcC}^*), \\ d_{fvcC}^*(x^*) & (L_{fvc}^* - \Delta L_{fvcC}^* \le x^* < L_{fvc}^*), \\ d_{fvcE}^*(x^*) & (x^* \ge L_{fvc}^*), \end{cases} \qquad (4)$$

where

Table 1 Size parameters of the glottis.

D_s^*	16.4 mm	ΔL_{fvcE}^*	3.0 mm
D_v^*	10.3 mm	a_-	3.0
D_f^*	5.1 mm	b_-	0.3
D_t^*	19.0 mm	c_-	2.0×10^{-2}
L_{fvc}^*	5.8 mm	a_+	17.0
ΔL_{fvcC}^*	3.8 mm	b_+	0.1

$$\left.\begin{aligned} &A_1^* = D_s^*,\ A_2^* = D_g^*, \\ &s(x^*) = \frac{a_-}{D^*}|x^* + D^* c_-| - \frac{D^* b_-}{|x^* + D^* c_-|}, \end{aligned}\right\} \quad (x^* \le 0),$$
$$\left.\begin{aligned} &A_1^* = D_v^*,\ A_2^* = D_g^*, \\ &s(x^*) = \frac{a_+}{D^*}|x^*| - \frac{D^* b_+}{|x^*|}, \end{aligned}\right\} \quad (x^* > 0), \qquad (5)$$

$$d_{fvcC}^*(x^*) = \frac{1}{2}(D_f^* - D_v^*)\left\{1 + \cos\left(\pi \frac{x^* - L_{fvc}^*}{\Delta L_{fvcC}^*}\right)\right\}, \qquad (6)$$

$$d_{fvcE}^*(x^*) = D_t^* - D_v^* + (D_f^* - D_t^*)\exp\left\{-\frac{1}{2}\left(\frac{x^* - L_{fvc}^*}{\Delta L_{fvcE}^*}\right)^2\right\}. \qquad (7)$$

The size parameters of the glottis in Eqs. (2)–(7) are indicated in Table 1 according to the data measured by Scherer *et al.* [13].

In the model, it is assumed that lung pressure can be described by an air reservoir at the boundary Γ_1 in Fig. 1, where the pressure is set to P_{in}^*.

In reality, speech production involves excitation of several acoustic modes within the vocal tract, i.e. formants. However, we assume herein that the vocal tract configuration is approximated by a uniform duct in order to highlight acoustic and fluid phenomena within the larynx. The effects of such acoustic loadings are ignored herein.

2.2. Governing Equations

Several studies have assumed the glottal flow to be incompressible [8,10,11], since, in general, the velocity of glottal flow ($\sim \mathcal{O}(10^0)$ m/s) is much slower than the speed of sound ($\simeq 350\,\mathrm{m/s}$), except at the exit of the glottis, and the pressure difference ($\sim \mathcal{O}(10^3)$ Pa) between the subglottal and supraglottal pressures is smaller than the atmospheric pressure ($\simeq \mathcal{O}(10^5)$ Pa). On the other hand, a jet-like flow with a velocity comparable to the sound velocity has been observed downstream of the glottis [5]. In addition, since the voice is a sound wave, i.e., an elastic wave in a fluid, the compressibility of the air should be important in the speech production phenomena. Therefore, in the present paper, we assume the glottal flow to be a compressible viscous fluid.

For a complicated configuration such as the glottis, shown in Fig. 1, it is difficult to specify the boundary

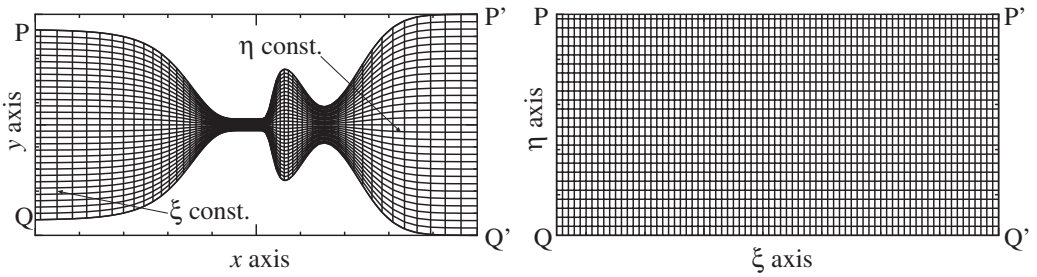

(a) Physical plane (x, y) (b) Computational plane (ξ, η)

Fig. 2 Transformation from the physical plane (x, y) to the computational plane (ξ, η) and the grids used in the numerical simulation.

conditions in Cartesian coordinates. Therefore, transformed general curvilinear coordinates (ξ, η) in Fig. 2 are obtained from the normalized Cartesian coordinates system (x, y) by

$$\begin{aligned} \xi &= \xi(x, y), \\ \eta &= \eta(x, y) = \frac{y + d_g(x)}{2d_g(x)}. \end{aligned} \tag{8}$$

The glottal flows, P, $\boldsymbol{u}$, ρ, and T, are numerically analyzed based on the rigid model shown in Fig. 1. The basic governing equations of hydrodynamics in a two-dimensional space (ξ, η), determined elsewhere, are summarized in the following compact form [14]:

$$\frac{\partial \boldsymbol{Q}}{\partial t} + \frac{\partial \boldsymbol{E}}{\partial \xi} + \frac{\partial \boldsymbol{F}}{\partial \eta} = \frac{1}{Re}\left(\frac{\partial \boldsymbol{R}}{\partial \xi} + \frac{\partial \boldsymbol{S}}{\partial \eta}\right), \tag{9}$$

where $Re = \rho_0^* c_0^* D^* / \mu_0^*$ is the Reynolds number, and μ_0^* is the shear viscosity. Other dependent variables for the flow field are expressed as

$$\boldsymbol{Q} = \frac{1}{J}\begin{bmatrix} \rho \\ \rho u \\ \rho v \\ e \end{bmatrix}, \tag{10}$$

$$\boldsymbol{E} = \frac{1}{J}\begin{bmatrix} \rho U \\ \rho u U + \xi_x P \\ \rho v U + \xi_y P \\ (e + P)U \end{bmatrix}, \boldsymbol{F} = \frac{1}{J}\begin{bmatrix} \rho V \\ \rho u V + \eta_x P \\ \rho v V + \eta_y P \\ (e + P)V \end{bmatrix}, \tag{11}$$

$$\boldsymbol{R} = \frac{1}{J}\begin{bmatrix} 0 \\ \xi_x \tau_{xx} + \xi_y \tau_{xy} \\ \xi_x \tau_{yx} + \xi_y \tau_{yy} \\ \xi_x \beta_x + \xi_y \beta_y \end{bmatrix}, \boldsymbol{S} = \frac{1}{J}\begin{bmatrix} 0 \\ \eta_x \tau_{xx} + \eta_y \tau_{xy} \\ \eta_x \tau_{yx} + \eta_y \tau_{yy} \\ \eta_x \beta_x + \eta_y \beta_y \end{bmatrix}. \tag{12}$$

Here, U and V are contravariant velocity components in the ξ and η directions, respectively, and are written as

$$\begin{aligned} U &= \xi_x u + \xi_y v, \\ V &= \eta_x u + \eta_y v. \end{aligned} \tag{13}$$

J is the Jacobian of the coordinate transformation

$$J = \frac{\partial(\xi, \eta)}{\partial(x, y)} = \begin{vmatrix} \dfrac{\partial \xi}{\partial x} & \dfrac{\partial \xi}{\partial y} \\ \dfrac{\partial \eta}{\partial x} & \dfrac{\partial \eta}{\partial y} \end{vmatrix} = \begin{vmatrix} \xi_x & \xi_y \\ \eta_x & \eta_y \end{vmatrix}, \tag{14}$$

and ξ_x, ξ_y, η_x, and η_y are the metrics. In the present study, for the relationship $\xi = \xi(x, y) = \xi(x)$ specified in Fig. 2, the metric ξ_y becomes zero, and so each component related to ξ_y in the governing equations Eqs. (11) and (12) can be partially simplified.

The dimensionless total energy density is given as

$$e = \frac{P}{\gamma - 1} + \frac{1}{2}\rho(u^2 + v^2), \tag{15}$$

where γ is the specific heat ratio. The dimensionless viscosity-induced drag forces in Eq. (12) are written as

$$\begin{aligned} \tau_{xx} &= \frac{2}{3}\mu\left(2\frac{\partial u}{\partial x} - \frac{\partial v}{\partial y}\right), \\ \tau_{yy} &= \frac{2}{3}\mu\left(2\frac{\partial v}{\partial y} - \frac{\partial u}{\partial x}\right), \\ \tau_{xy} &= \tau_{yx} = \mu\left(\frac{\partial u}{\partial y} + \frac{\partial v}{\partial x}\right), \end{aligned} \tag{16}$$

$$\begin{aligned} \beta_x &= \tau_{xx} u + \tau_{xy} v + \frac{\kappa}{(\gamma - 1)Pr}\frac{\partial T}{\partial x}, \\ \beta_y &= \tau_{yx} u + \tau_{yy} v + \frac{\kappa}{(\gamma - 1)Pr}\frac{\partial T}{\partial y}. \end{aligned} \tag{17}$$

Here, $\mu = \mu^*/\mu_0^*$ and $\kappa = \kappa^*/\kappa_0^*$ are the dimensionless shear viscosity and thermal conductivity, respectively. $Pr = c_p^* \mu_0^* / \kappa_0^*$ is the Prandtl number, and c_p^* is the specific heat coefficient at a constant pressure. Operators $\partial/\partial x$ and $\partial/\partial y$ in Eqs. (16) and (17) are described as

$$\begin{aligned} \frac{\partial}{\partial x} &= \xi_x \frac{\partial}{\partial \xi} + \eta_x \frac{\partial}{\partial \eta}, \\ \frac{\partial}{\partial y} &= \xi_y \frac{\partial}{\partial \xi} + \eta_y \frac{\partial}{\partial \eta} = \eta_y \frac{\partial}{\partial \eta}. \end{aligned} \tag{18}$$

The viscosity and the thermal conductivity in air depend primarily on temperature. Thus, the semiempirical formulae proposed by Sutherland [15]:

$$\mu = \frac{T_0^* + T_S^*}{T_0^* T + T_S^*} T^{3/2}, \qquad \kappa = \frac{T_0^* + T_A^* e^{-T_B^*/T_0^*}}{T_0^* T + T_A^* e^{-T_B^*/(T_0^* T)}} T^{3/2}, \tag{19}$$

are then utilized, where $T_S^* = 110.4\,\mathrm{K}$, $T_A^* = 245.4\,\mathrm{K}$, and $T_B^* = 27.6\,\mathrm{K}$.

In addition, an adiabatic relationship for a compressible fluid is used to related the absolute temperature and the pressure

$$P = \frac{\rho T}{\gamma}. \tag{20}$$

Since the governing equations, Eqs. (9)–(12), are nonlinear partial differential equations, solving these equations analytically subject to initial and boundary conditions is extremely involved. Instead, we employ a numerical computation method, MacCormack's finite-difference scheme [16,17], which has forth-order accuracy with respect to space and second-order accuracy with respect to time.

2.3. Initial and Boundary Conditions

Suppose that the air in the larynx is uniform and at rest for $t \le 0$. Then, the initial conditions are readily obtained for the entire space of the larynx and the vocal tract

$$|\boldsymbol{u}| = 0, \quad \rho = 1, \quad P = 1/\gamma \quad (t \le 0), \tag{21}$$

where $1/\gamma$ is the nondimensional atmospheric pressure.

The boundary conditions for $t > 0$ are given below. Non-slip and adiabatic conditions are specified on the boundaries Γ_3 and Γ_4 in Fig. 1. At the surfaces of the vocal cords, the velocity of the fluid becomes zero due to the existence of viscosity. Furthermore, a non-reflecting characteristic boundary condition [18] is imposed at the outflow boundary Γ_2 in order to minimize acoustic reflection. In reality, although speech waves within the vocal tract involve forward ($+x$) and backward ($-x$, reflecting) waves, which interfere with each other, we ignore such reflecting waves, since our focus in the present study is on the fluid motion within the glottis. A pressure function $P_{\mathrm{in}}(t) = p_{\mathrm{L}}(t) + 1/\gamma$ is applied to the boundary Γ_1, where $p_{\mathrm{L}}(t)$ is the lung pressure,

$$p_{\mathrm{L}}(t) = \begin{cases} \dfrac{P_{\mathrm{L0}}}{2}\left\{1 - \cos\left(\dfrac{\pi t}{t_{\mathrm{r}}}\right)\right\} & (0 < t \le t_{\mathrm{r}}), \\ P_{\mathrm{L0}} & (t > t_{\mathrm{r}}). \end{cases} \tag{22}$$

$P_{\mathrm{L0}}(= P_{\mathrm{L0}}^*/(\rho_0^* c_0^{*2}))$ and $t_{\mathrm{r}}(= c_0^* t_{\mathrm{r}}^*/D^*)$ are the steady-state value of $p_{\mathrm{L}}(t)$ and the time required for $p_{\mathrm{L}}(t)$ to increase to P_{L0} from zero (referred to as the rise time), respectively.

2.4. Analysis Conditions

A computational domain extends from $x = -8$ to $x = 10$, i.e. $x^* = -150\,\mathrm{mm}$ to $x^* = 190\,\mathrm{mm}$. An integration region is divided into 800 grids along the ξ direction and 120 grids along the η direction, as shown in Fig. 2(a). The method used to decide these grid numbers is discussed in the Appendix.

The dimensions of the grids in the x direction are reduced near the vocal cords at $x = 0$, and the grids in the y direction are regular. Here, the minimum grid sizes become $\Delta x^* \simeq 40\,\mu\mathrm{m}$ and $\Delta y^* \simeq 8\,\mu\mathrm{m}$. The physical parameters used in this study are listed in Table 2. In the present paper, the rise time is set to a constant value of $t_{\mathrm{r}}^* = 10\,\mathrm{ms}$.

Table 2 Physical parameters (37°C, 1 atm).

c_0^*	Speed of sound	$3.532 \times 10^2\,\mathrm{m/s}$
ρ_0^*	Density of the medium	$1.138\,\mathrm{kg/m^3}$
μ_0^*	Shear viscosity	$1.902 \times 10^{-5}\,\mathrm{Pa{\cdot}s}$
κ_0^*	Thermal conductivity	$2.530 \times 10^{-2}\,\mathrm{W{\cdot}m^{-1}{\cdot}K^{-1}}$
c_{p}^*	Specific heat coefficient at constant pressure	$1.006 \times 10^3\,\mathrm{J{\cdot}K^{-1}{\cdot}kg^{-1}}$
γ	Specific heat ratio	1.403

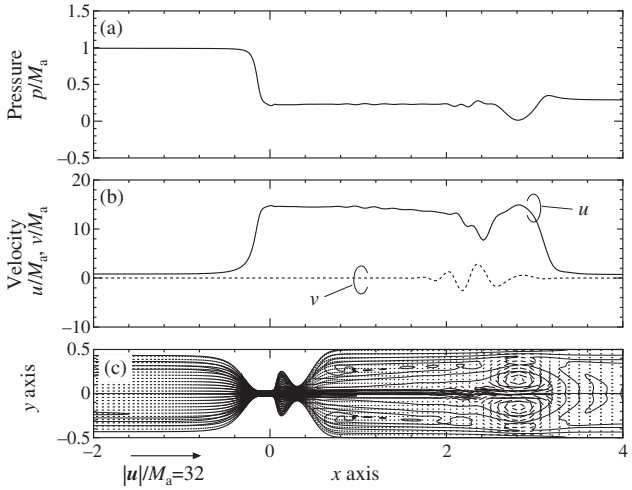

Fig. 3 Glottal flow distribution at $t^* = 10\,\mathrm{ms}$. Pressure (a) and flow velocity (b) distributions along the x axis. Vorticity and flow vector distributions in the larynx are shown in (c), in which the straight-line segments denote glottal flow vectors and the contour lines denote the z components of the vorticity. $P_{\mathrm{L0}}^* = 1{,}000\,\mathrm{Pa}$ and $D_{\mathrm{g}}^* = 1\,\mathrm{mm}$.

3. RESULTS

3.1. Flow Pattern in the Glottis

The flow pattern in the glottis at $t^* = 10\,\mathrm{ms}$ is shown in Fig. 3. The gap distance between the vocal cords D_{g}^* is 1 mm, and the lung pressure P_{L0}^* is set to 1,000 Pa, which corresponds to the value on a middle conversation level.

The one-dimensional distributions of pressure $p = P - 1/\gamma$ and velocities u and v along the x axis ($y = 0$) are shown in Figs. 3(a) and (b), respectively. The results near the glottis in the range of $x = -2$ to $x = 4$ are only plotted in Fig. 3, although we computed the flow in the range of

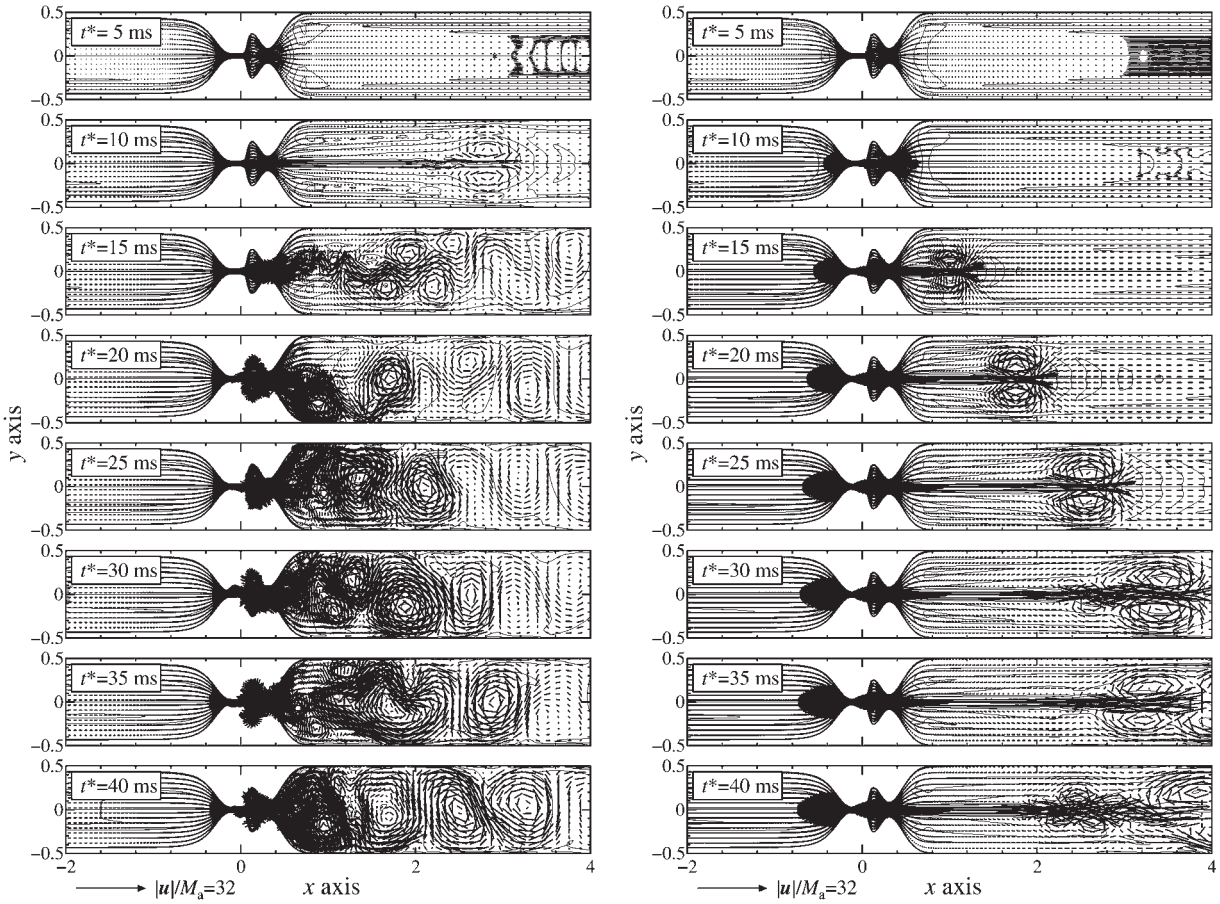

Fig. 4 Time sequences of the glottal flow pattern for $D_g^* = 1$ mm. Straight-line segments denote glottal flow vectors, and contour lines denote the z components of the vorticity.

$x = -8$ to $x = 10$. Each value is normalized by $M_a = P_{L0}^*/(\rho_0^* c_0^{*2})$. The maximum values of pressure and velocity correspond to approximately 1,000 Pa and 38 m/s, respectively. A sudden pressure drop occurred at the glottal entrance $x \simeq -0.2$, due to a flow acceleration, and a main flow in the x direction was generated from $x = 0$ to 3. A two-dimensional glottal flow pattern is shown in Fig. 3(c). The straight-line segments represent glottal flow vectors, and the contour lines denote the z components of vorticity

$$\boldsymbol{\omega} = \nabla \times \boldsymbol{u}, \tag{23}$$

which is a measure of angular velocity. The jet-like flow pattern was approximately symmetric about the x axis and was concentrated on the x axis.

Figure 4 shows the time sequences of a two-dimensional glottal flow with a gap $D_g^* = 1$ mm. In order to examine glottal flows under both phonation and non-phonation conditions, the lung pressure P_{L0}^* in (a) is set to 1,000 Pa above the phonation threshold pressure, which is usually from 300 to 400 Pa, and that in (b) is set to 100 Pa below the phonation threshold pressure. For $P_{L0}^* = 1{,}000$ Pa, although a symmetric jet was observed for $t^* < 10$ ms, several vortices were generated within the flow for $t^* > 15$ ms and the structure of the jet became asymmetric. Furthermore, comparatively large vortices were generated downstream of the glottis $0 < x < 2$, and the structure of vortices indicated unsteady patterns that changed with time. On the other hand, for the condition of $P_{L0}^* = 100$ Pa, the flow was a jet-like structure having two vortices and a symmetric pattern for $t^* = 0$–30 ms. The jet for $t^* > 50$ ms at $P_{L0}^* = 100$ Pa is finally translated into an asymmetric flow similar to that at 1,000 Pa.

The vortices in the flow shown in Fig. 4 at $t^* = 30$ ms are shown in Fig. 5 with expanded coordinates. The flow at 1,000 Pa is not parallel to the x axis and is skewed toward the side for $y < 0$ near the glottis ($x \simeq 0.3$), and several vortices are observed. Although the jet shifted toward $y < 0$ at 30 ms, after that the jet angle changed with time between the sides for $y < 0$ and > 0. The contour lines of vortices are concentrated within the ventricle of the larynx, and the glottal jet, which impinges on the false vocal cord, is mainly formed for $0 < x < 0.5$. Furthermore, the length of the jet is approximately consistent with the distance between the true and false vocal cords. In contrast, the

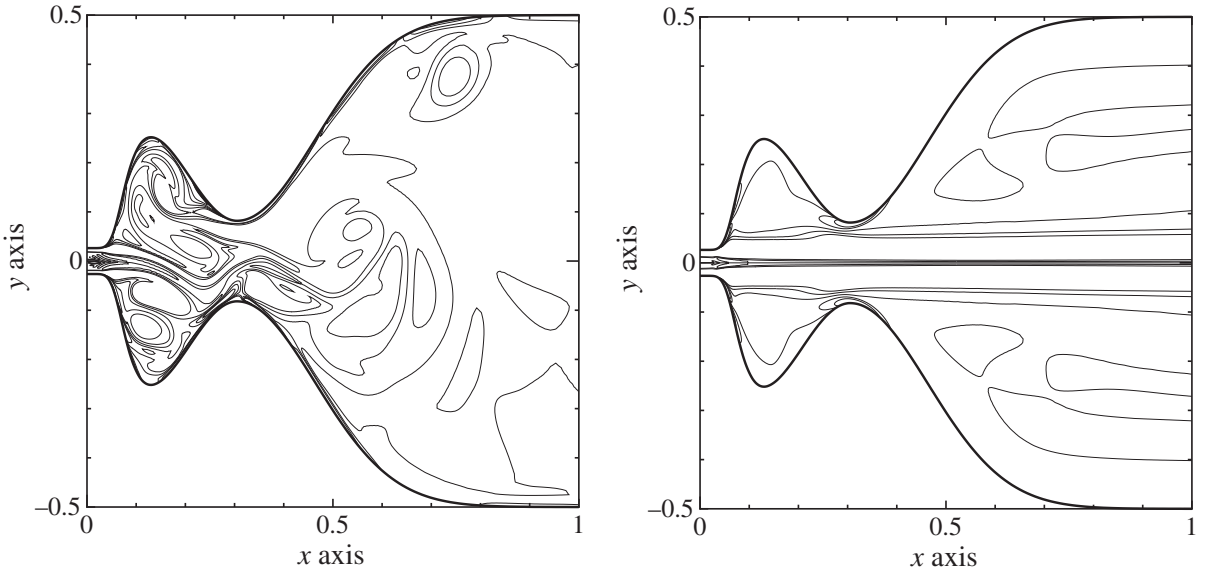

Fig. 5 Glottal flow patterns at the exit of the glottis at $t^* = 30$ ms for $D^*_g = 1$ mm. The contour lines denote the z components of the vorticity. The flow is identical to that shown in Fig. 4 at $t^* = 30$ ms (shown with expanded coordinates).

contour of the vortices at 100 Pa in (b) indicate that the flow is ejected from the glottis parallel to the x axis.

The results indicate that the glottal flow initially has a symmetric jet structure with vortices at the flow front, after which the structure of the vortices becomes asymmetric, and the flow pattern changes with time.

3.2. Pressure Fluctuations in the Flow

Next, we measured the instantaneous pressure of the flow at fixed points in order to examine behavior of the unsteady glottal flow. Normalized nondimensional pressure at different distances from the glottis for $D^*_g = 1$ mm and $P^*_{L0} = 1{,}000$ Pa are shown in Fig. 6. Pressure fluctuations were generated at all observation points. In particular, the fluctuations at $x = 0$, 1, and 2 for $t^* > 10$ ms were remarkable. The transient time at which the pressure began to fluctuate was nearly equal to the time of translation from the simple jet into the asymmetric flow in Fig. 4(a).

Figure 7 shows the pressures measured at $x = 2$ and $y = 0$ for the glottis $D^*_g = 1$ mm at $P^*_{L0} = 1{,}000$ and 100 Pa. The fluctuation component at 100 Pa was less than that at 1,000 Pa.

These results indicate that the fluctuations tend to decrease with the distance from the glottis and increase with lung pressure.

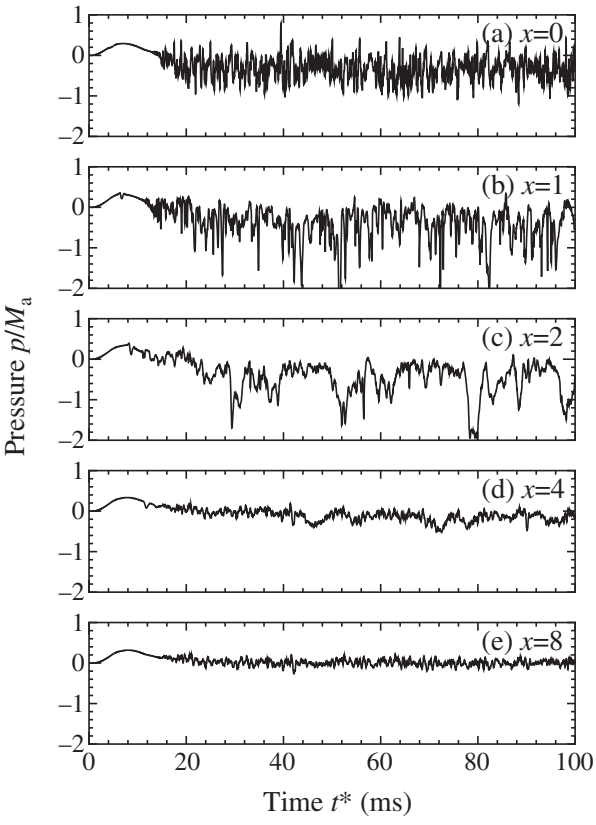

Fig. 6 Pressure in the glottal flow at $y = 0$ for $P^*_{L0} =$ 1,000 Pa and $D^*_g = 1$ mm.

4. DISCUSSION

In the previous section, we indicated the unsteady glottal flow and the asymmetric structure thereof. Similar results have been obtained by Iijima *et al.* [10], and they conjectured that an observed asymmetry was due to numerical errors in a computation. Therefore, let us discuss whether the asymmetric flow based on the static glottal

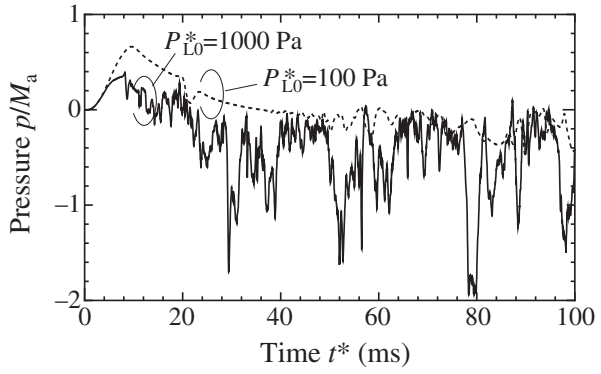

Fig. 7 Effect of lung pressure on pressure for $D^*_g = 1$ mm. Pressures are measured at $x = 2$, $y = 0$.

model is an essential phenomenon in physics or is perhaps caused by numerical errors in computation.

It is possible that asymmetrical numerical computation could cause asymmetric flow. In order to avoid such an asymmetry, we used forward and backward differences in differential operations at alternate time steps. Furthermore, we have compared the numerical and analytical solutions of the Poiseuille flow [19] in order to verify our numerical method, and both results were in good agreement and indicated symmetric flows. In addition, a numerical flow having an orifice with one half width of the duct was calculated in order to verify the stability for the boundary shape. The obtained result indicates that the flow with vortices remained symmetric for a long computational time ($t^* < 1$ s).

On the other hand, a flow instability can be determined using the Reynolds number. A critical Reynolds number exists, beyond which a flow is unstable, and this Reynolds number is determined by, for example, the geometry of duct or the scale of the disturbance in the flow. Therefore, in the present numerical experiments, we estimate the Reynolds number Re_g at the glottis. We define the Reynolds number as $Re_g = \rho^*_0 |\boldsymbol{u}^*_{max}| D^*_g / \mu^*_0$, where $\boldsymbol{u}^*_{max}$ is the maximum velocity of the flow within the glottis. The obtained Reynolds numbers are listed in Table 3. Since critical Reynolds numbers of the glottal flow are unknown, we compared the obtained values of $\mathcal{O}(10^3)$ with the general critical Reynolds number of $\mathcal{O}(10^0) \sim \mathcal{O}(10^3)$ [20]. The comparison indicates that the obtained Reynolds numbers are not much greater than the general critical Reynolds number. However, the obtained Reynolds numbers are sufficient to translation from a steady and stable flow to an unsteady and unstable flow. Therefore, the transition to an asymmetric flow is physically plausible, and numerical errors do not affect the asymmetric flow.

Table 3 Reynolds numbers at the glottis.

Lung pressure P^*_{L0} (Pa)	Reynolds number Re_g
1,000	2.9×10^3
100	8.7×10^2

Liljencrants has also reported asymmetric flows obtained in numerical simulations based on a rigid glottal model [11]. However, he did not examine whether the asymmetry was only a transient phenomenon of the flow or the flow had completely translated into an unsteady flow. Therefore, the present study is important because we have demonstrated that the glottal flow eventually translates into unsteady and asymmetric flow. Although he assumed the glottal flow to be incompressible, asymmetric flow was obtained in the larynx as well as that in the present study. This result indicates that the asymmetric glottal flows do not depend on the assumption of compressible or incompressible flows. The effect of the compressibility of air on speech production remains a topic for further discussion.

We next compare the numerical flow obtained by the present simulation with measured flows through a rigid glottis. Hofmans *et al.* [8] and Pelorson *et al.* [9] have measured flows based on rigid models having lip-like or divergent glottises without false vocal cords.

In their experiments, instantaneous pressures measured at the glottis also indicated fluctuations. However, the amplitude of pressure fluctuation calculated by the our numerical analysis is greater than that measured in their experiment. The pressure fluctuations (peak to peak values) at the smallest aperture of the constriction in the present study and in their experiment are 1 and 0.5 times lung pressure, respectively.

The discrepancy in the pressure fluctuations may be due to the difference of model configuration, in other words, the numerical glottal model has the false vocal cords whereas the physical models do not. A result related to the false vocal cords of the numerical simulation is that the length of the jet was approximately consistent with distance between the true and false vocal cords. Figure 5(a) shows that the impingement of the flow on the false vocal cords causes vortices in the ventricle of larynx. Circulating these vortices in the ventricle of the larynx, a small and local instability of the flow transforms into a greater and more global phenomenon with time. In order to confirm this hypothesis, we compared numerical glottal flows based on models with and without false vocal cords. Measured instantaneous pressure at the glottis, $x = 0$, for $D^*_g = 1$ mm and $P^*_{L0} = 1{,}000$ Pa are showed in Fig. 8. This result indites that the normalized pressure fluctuation is about 1 on the model with false vocal cords, while the fluctuation is about 0.5 on the model without false vocal cords. Therefore, it is concluded that the difference of pressure fluctuations between results on the numerical and measured glottal flow is caused by the existence of the false vocal

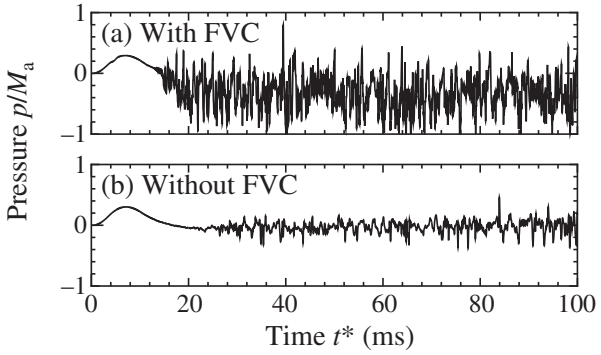

Fig. 8 Effect of the FVC (False Vocal Cords) on pressure at $x = 0$ and $y = 0$ for $D_g^* = 1$ mm and $P_{L0}^* = 1{,}000$ Pa.

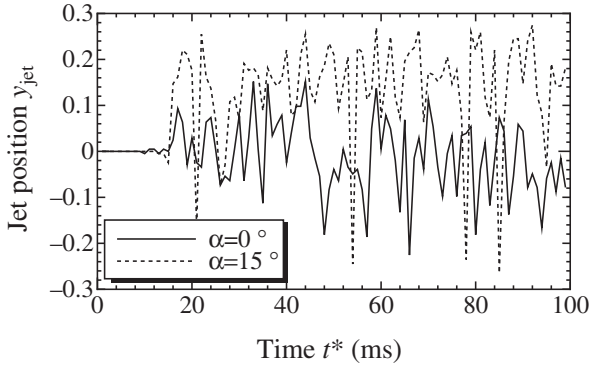

Fig. 9 Effect of divergent angle α on the glottal flow. The jet position y_{jet} at $x = 0.5$ is plotted as function of time for $D_g^* = 1$ mm and $P_{L0}^* = 1{,}000$ Pa. The jet position is estimated from the position at which the glottal flow velocity u indicates the maximum value.

cords. Furthermore, the value based on the numerical model without false vocal cords is consistent with the value measured by Hofmans *et al.* [8], therefore, the verification of our numerical simulation is confirmed.

Glottal flows in static models have been visualized by Shinwari *et al.* [5] and Pelorson *et al.* [9]. Both results showed that glottal jets were not symmetric about the main flow direction and skewed toward each side. These results were also obtained in the numerical experiments of the present study. This indicates that a one-dimensional model, which assumes the flow distribution in the direction perpendicular to the main flow to be uniform, is inappropriate for the analysis of a complicated glottal flow with several vortices and asymmetry. This conclusion is supported by our numerical simulation, which showed symmetric vortices based on the two-dimensional larynx model.

We indicated earlier that the fluctuation of pressure obtained in the numerical simulation of the present study was larger than that measured by Hofmans *et al.* [8]. Another difference between the simulation and measurement results is that the asymmetric jets obtained by the measurement were quite steady, whereas the numerical jets formed unsteady flow patterns. When the glottal flows in the visualization were skewed toward the each side at some angle, the angle of the jet was not changed and a stationary pattern was formed [5], although the numerical jet indicated unsteady flow patterns and an unsteady oblique angle which varied in direction with time for $y < 0$ and > 0. In general, the generation of skewed jets, namely the Coanda effect, requires steady flow conditions and the existence of a diffuser with a divergent angle greater than approximately 10 degrees [21]. Under these conditions, a small perturbation in shear layer at the glottis causes the Coanda effect. Therefore, the Coanda effect did not occur in the present numerical experiment, because the model is based on the parallel glottal model with a divergent angle of 0 degrees.

In order to examine effects of divergent angle α on the glottal flows, we compared the numerical jets through the glottis with the divergent angle $\alpha = 0$ and 15 degrees. Figure 9 shows the jet position in the y direction, y_{jet}, at $x = 0.5$ as function of time for $D_g^* = 1$ mm and $P_{L0}^* = 1{,}000$ Pa. The jet position is estimated from the position at which the glottal flow velocity u indicates the maximum value. The result of jet position for $\alpha = 15$ degrees indicates that the direction of jet is almost fixed for $y > 0$, i.e. the generation of Coandar effect, although the position of jet for $\alpha = 0$ degrees changes between $y < 0$ and $y > 0$, in other words, the jet position shows the unsteady motion with change of jet angle with time. From this result, it is conclude that the unsteady glottal flow with the change of jet angle is a characteristic motion in the parallel model.

5. CONCLUSION

We have numerically simulated the glottal flow based on a two-dimensional model in order to examine behavior of unsteady flow within the larynx. Although the glottal sound source has been described as the interaction between the flow and the vibrating vocal cords, in order to focus on only fluid motion, we herein assumed the vocal cords to be non-vibrating rigid bodies.

The nonlinear hydrodynamics equations for a compressible viscous fluid were integrated using MacCormack's finite-difference scheme. The simulation yielded the following results: (1) the initial flow was a jet-like stream with two vortices and a symmetric pattern about the x axis, (2) after which the structure of the vortices became asymmetric and the flow was translated into a complicated pattern that changed with time, and (3) the pressure in the glottal flow began to fluctuate sharply, and increases in the lung pressure resulted in larger fluctuations. In summary, rather than being a steady symmetric laminar flow, the glottal

flow is an unsteady complicated flow having a structure that changes with time. In addition, the results of the present study suggest that simple assumptions, such as linearization of the fluid equations in the speech production process and a one-dimensional glottal model, are not appropriate for analysis of the speech production process. Furthermore, we indicated that the asymmetric glottal flow in computation is not caused by numerical errors and is valid physical phenomena.

In the present paper, we have demonstrated that the glottal flow became unsteady with time. As such, several numerical experiments and quantitative analyses based on the present model are necessary in order to discuss the relationship between unsteady flows and speech waves. The effects of unsteady flow on the glottal sound source remains unclear and should be discussed further.

ACKNOWLEDGMENTS

This research was partially supported by the Nakatani Electronic Measuring Technology Association of Japan.

REFERENCES

[1] K. Ishizaka and J. L. Flanagan, "Synthesis of voiced sounds from a two-mass model of the vocal cords," *Bell Syst. Tech. J.*, **51**, 1233–1268 (1972).
[2] B. H. Story and I. R. Titze, "Voice simulation with a body-cover model of the vocal folds," *J. Acoust. Soc. Am.*, **97**, 1249–1260 (1997).
[3] S. Adachi and J. Yu, "Two-dimensional model of vocal fold vibration for sound synthesis of voice and soprano singing," *J. Acoust. Soc. Am.*, **117**, 3213–3224 (2005).
[4] J. van den Berg, J. T. Zantema and P. Doorenbal, "On the air resistance and the Bernoulli effect of the human larynx," *J. Acoust. Soc. Am.*, **29**, 626–631 (1957).
[5] D. Shinwari, R. C. Scherer, K. J. DeWitt and A. A. Afjeh, "Flow visualization and pressure distributions in a model of the glottis with a symmetric and oblique divergent angle 10 degrees," *J. Acoust. Soc. Am.*, **113**, 487–497 (2003).
[6] F. Alipour and R. C. Scherer, "Pressure and velocity profiles in a static mechanical hemilarynx model," *J. Acoust. Soc. Am.*, **112**, 2996–3003 (2002).
[7] R. C. Scherer, D. Shinwari, K. J. De Witt, C. Zhang, B. R. Kucinsche and A. A. Afjeh, "Intraglottal pressure profiles for a symmetric and oblique glottis with a divergence angle of 10 degrees," *J. Acoust. Soc. Am.*, **109**, 1616–1630 (2001).
[8] G. C. J. Hofmans, G. Groot, M. Ranucci, G. Graziani and A. Hirschberg, "Unsteady flow through *in-vitro* models of the glottis," *J. Acoust. Soc. Am.*, **113**, 1658–1675 (2003).
[9] X. Pelorson, A. Hirschberg, A. P. Wijnands and H. Bailliet, "Description of the flow through *in-vitro* models of the glottis during phonation," *Acta Acustica*, **3**, 191–202 (1995).
[10] H. Iijima, N. Miki and N. Nagai, "Glottal impedance based on a finite element analysis of two-dimensional unsteady viscous flow in a static glottis," *IEEE Trans. Signal Process.*, **40**, 2125–2135 (1992).
[11] J. Liljencrants, "Numerical simulations of glottal flow," *STL-QPSR*, 1/1989, 69–74 (1989).
[12] C. Zhang, W. Zhao, S. H. Frankel and L. Mongeau, "Computational aeroacoustics of phonation, Part II: Effects of flow parameters and ventricular folds," *J. Acoust. Soc. Am.*, **112**, 2147–2154 (2002).
[13] R. C. Scherer, I. R. Titze and J. F. Curtis, "Pressure-flow relationships in two models of the larynx having rectangular glottal shapes," *J. Acoust. Soc. Am.*, **73**, 668–676 (1983).
[14] J. C. Tannehill, D. A. Anderson and R. H. Pletcher, *Computational Fluid Mechanics and Heat Transfer*, 2nd ed. (Taylar & Francis, Washington DC, 1997), Sect. 5.1, pp. 249–271.
[15] A. D. Pierce, *Acoustics* (Acoustical Society of America, New York, 1989), Sect. 10.1, pp. 513–514.
[16] E. Turkel, "On the practical use of high-order methods for hyperbolic systems," *J. Comput. Phys.*, **35**, 319–340 (1980).
[17] [14], Sect. 9.2, pp. 622–641.
[18] T. J. Poinsot and S. K. Lele, "Boundary conditions for direct simulations of compressible viscous flows," *J. Comput. Phys.*, **101**, 104–129 (1992).
[19] L. D. Landau and E. M. Lifshitz, *Fluid Mechanics*, 2nd Ed. (Pergamon Press, Oxford, 1987), Sect. 17, pp. 51–54.
[20] [19], Sect. 26, pp. 95–99.
[21] S. J. Kline, D. E. Abbott and R. W. Fox, "Optimum design of straight-walled diffusers," *Trans. ASME Ser. D J. Basic Eng.*, **81**, 321–331 (1954).

APPENDIX

In finite difference methods, the accuracy of numerical solutions depends on the grid numbers. The values used in the present study were determined as follows. Glottal flows were numerically calculated for various grid number by varying M in the ξ direction and N in the η direction. The grid numbers at which the obtained numerical values were saturated were used to for the computations.

Table A.1 shows the simulated pressures of glottal flow at grid numbers of $M = 460$ and 800 and $N = 60$ and 120 based on the rigid model with gap $D_g^* = 1\,\mathrm{mm}$. The table indicates the normalized non-dimensional pressure fluctuations P_{rms}/M_as at $x = 2$. The pressure values for the 800×60 and 800×120 grids show approximately the same. Therefore, the grid numbers are determined as $M = 800$ and $N = 120$.

Table A.1 Relationship between grid numbers M and N and root-mean-squared values of nondimensional pressure fluctuations P_{rms}. M and N are the grid numbers in ξ and η directions, respectively. The pressure fluctuation is measured at $x = 2$ for $P_{L0}^* = 1{,}000\,\mathrm{Pa}$.

Grid number $M \times N$	Pressure P_{rms}/M_a
460×60	2.2×10^{-1}
460×120	2.5×10^{-1}
800×60	5.0×10^{-1}
800×120	4.4×10^{-1}